Applied Energy 298 (2021) 117245

Contents lists available at ScienceDirect

Applied Energy

journal homepage: www.elsevier.com/locate/apenergy

# A hybrid solution for offshore wind resource assessment from limited onshore measurements

Basem Elshafei [a], Alfredo Peña [b], Dong Xu [c], Jie Ren [a], Jake Badger [b], Felipe M. Pimenta [d], Donald Giddings [a], Xuerui Mao [a,*]

[a] Faculty of Engineering, University of Nottingham, NG7 2RD, Nottingham, UK
[b] DTU Wind Energy, Technical University of Denmark, Roskilde, Denmark
[c] Xinjiang Goldwind Science and Technology Co., Ltd, PR China
[d] Centro de Ciencias Fisicas e Matematicas, Campus Trindade, Universidade Federal de Santa Catarina Florianopolis, SC 88010-970, Brazil

## GRAPHICAL ABSTRACT

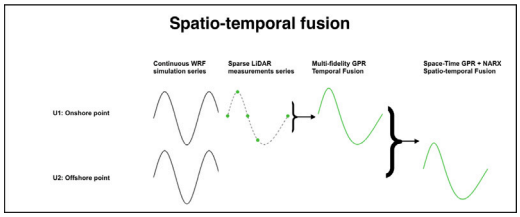


## ARTICLE INFO

*Keywords:*
Artificial neural network
Gaussian process regression
Spatiotemporal data fusion
Wind resource assessment

## ABSTRACT

In wind resource assessments, which are critical to the pre-construction of wind farms, measurements by LiDARs or masts are a source of high-fidelity data, but are expensive and scarce in space and time, particularly for offshore sites. On the other hand, numerical simulations, using for example the Weather Research and Forecasting (WRF) model, generate temporally and spatially continuous data with relatively low-fidelity. A hybrid approach is proposed here to combine the merit of measurements and simulations for the assessment of offshore wind. Firstly a temporal data fusion using deep Multi Fidelity Gaussian Process Regression (MF-GPR) is performed to combine the intermittent measurement and the continuous simulation data at an onshore location. Then a spatial data fusion using a neural network with Non-linear Autoregression (NAR) and Non-linear Autoregression with external input (NARX) are conducted to project the wind from onshore to offshore. The numerical and measured wind speeds along the west coast of Denmark were used to evaluate the method. We show that the proposed data fusion technique using a gappy onshore measurement results in accurate offshore wind resource assessment within a 2% margin error.

## 1. Introduction

In the past decades, there has been worldwide demand for renewable energy, leading to a dramatic expansion in all its sectors, with a significant fraction generated by wind. There are over 230 GW of installed wind capacity in Europe as of 2020, consisting of 190 GW onshore and 40 GW offshore. Additionally, Europe intends to further the rise in demand for wind energy and its capacity by 35% [1]. Before the construction of a wind farm, it is critical to evaluate the wind speed condition of the location. Since the power is the cube function of wind speed, minor speed changes can cause large deviations in the output power. Moreover, the wind varies both geographically and temporally over a wide range of scales. Therefore, an accurate assessment of the wind resource for a proposed site is highly essential and is considered of paramount significance for a wind project to be successful [2,3].

* Corresponding author.
*E-mail address:* xuerui.mao@nottingham.ac.uk (X. Mao).

https://doi.org/10.1016/j.apenergy.2021.117245
Received 27 February 2021; Received in revised form 16 May 2021; Accepted 7 June 2021
Available online 15 June 2021

The assessment also helps to the selection of wind turbines and their layouts [4].

Physical wind measuring devices include e.g. LiDARs, meteorological mast towers, Satellite Synthetic Aperture Radars (SARs), and so forth. These equipment yield accurate results but are expensive and the data is commonly sparse in space and time. For example, the SARs measured wind is at 10 m above the sea surface with low temporal resolution and only applies to offshore assessments; LiDARs measure the Line-Of-Sight (LOS) velocity by computing the Doppler shift of the signal of an infrared laser beam based on the movement of aerosols and the output is usually intermittent at a fixed location; buoy systems are expensive and require regular maintenance, redundant systems for power, measurements, and communication for the measurement at a given location. On the contrary, numerical simulations result in wind predictions that cover large geographical areas and long time horizons continuously, but with relatively low fidelity. The numerical models include e.g. Weather Research and Forecasting (WRF), Global Forecast System (GFS), and European Centre for Medium-Range Weather Forecasts (ECMWF) [5].

Such a clear complement of physical measurements and numerical information suggests data fusion or a hybrid technique to combine the merit of both. It would be very desirable to extend the information from coastal online vertical LiDARs for the reconstruction of offshore time series as they are easier to maintain [6]. This technique can be used to numerically extend the information from coastal measurements to the offshore time series with low cost and high accuracy. Such techniques have been widely used in the prediction of future developments based on various inputs [7]. For example, Hu and Wang [8] used Empirical Wavelet Transforms (EWT), Partial Auto-Correlation Function (PACF), and GPR for wind speed assessments. EWT was employed to extract the meaningful data from the wind speed series through a customized wavelet filter bank, and PACF provided the input parameters for the GPR to simulate dynamic features and internal uncertainties. An alternative combination, i.e. Auto-Regressive (AR) and GPR, was followed by Zhang and Wei [6]. AR was employed to capture the structure of the wind speed series, and GPR to extract the local structures. As a supplement, Automatic Relevance Determination (ARD) considered the importance of using different inputs; thus, various types of covariance functions were combined to comprehend the characteristics of the data. This hybrid method outperformed others including Support Vector Machine (SVM), Artificial Neural Network (ANN), and the persistence approach. Meanwhile, an improved near-surface wind speed prediction experiment, which considered the atmospheric stability using GPR combined with Numerical Weather Prediction (NWP), for a time horizon of 72 h, showed that the consideration of atmospheric stability was able to reduce the estimated errors, thus improving power predictions [2].

Most recently, the Multi-Fidelity Gaussian Process Regression (MF-GPR) has been demonstrated to significantly outperform the regular single fidelity model. The strategy of MF-GPR was to go beyond the regular AR kriging scheme and introduce more than one data set at different fidelity levels. The first is a high-fidelity, scarce data set which can be the physically measured one; the second is a low-fidelity, continuous data set which can be generated from numerical simulations. The literature in this area further discussed various developments; for example, the Deep MF-GPR with additional data sets, e.g. first and second derivatives, phase-shifted oscillations, and different periodicity data sets leading to drastically improved approximations [9].

Further, wind resource assessments are commonly requested over a long-time-interval (e.g. a few months or years) and to cover large areas, therefore requiring spatial–temporal fusion of numerically and physically measured wind [10]. Apart from the temporal prediction reviewed above, ANNs are trained and tested on data sets from two different locations. Cadenas and Rivera, considered the problem of non-linearity in the time-series using Nonlinear Auto-Regressive with Exogenous inputs (NARX) [11]. The method was compared with both the persistence approach and Nonlinear Auto-Regressive (NAR). The results demonstrated that the NARX model was the most precise of the three and justified the extra input, suggesting that it could be suitable for spatial data fusion.

Spatiotemporal models which combine the aforementioned temporal and spatial fusion, have been widely used in the geostatistics field, where temperature and wind speed were the main variables of concern. In these models, the temporal extrapolation is performed to predict the values out of the measured interval at a fixed spatial point [12], followed by spatial extrapolation to project the estimation to a different point [13]. This sequential extrapolation in time and space was developed in the present study for wind resource assessment. Temporal data fusion of low and high-fidelity data from simulations and measurements at a given location was performed using deep MF-GPR, and spatial data fusion using a customized nonlinear autoregressive ANN with exogenous inputs was conducted thereafter. As illustrated in Fig. 1, the low fidelity results (e.g from numerical simulations) are assumed to be available across a continuous domain $X \times T$, where $X$ and $T$ are the spatial and temporal domains, respectively. On the other hand, high-fidelity results (e.g from the LiDAR measurements) are available in a reduced domain $X_{re} \times T_{re}$ where $X_{re}$ is a subset of $X$ and can be discontinuous and $T_{re}$ is a subset of $T$ and can be discontinuous. Thereafter, the objective was to combine the low and high-fidelity results to reach a data fusion on the full domain $X \times T$.

The novelty of this work lies on the development of a hybrid algorithm for the accurate assessment of offshore wind resources with reduced cost. It combines the generally continuous but low-fidelity numerical data and high-fidelity but limited physical measurements. Efforts were also devoted to pre-processing the time series and taking into account additional information not considered in existing methods to lift the accuracy of the fusion. This algorithm enables the projection of limited onshore measurements to offshore locations in light of numerical simulations with significantly higher accuracy than the industry standard approach.

This paper is organized as follows. In Section 2, we show details for our methodology for the temporal extrapolation using multi-fidelity GPR, and spatial extrapolation using NARX algorithms. In Section 3, we describe the case to be studied and the collection of the high and low fidelity data. In Section 4, we address the pre-processing technique used to smooth the given wind speed time-series. In Section 5, we present the main results and compare the performance of our methods against the industrial standard before drawing conclusions in Section 6.

## 2. Methodology

### 2.1. Temporal data fusion

In this section, we introduce the algorithms for temporal data fusion by combining the low-fidelity continuous time series and the high-fidelity intermittent one. The prototype of the Gaussian process regression is briefly introduced in Section 2.1.1 and then multi-fidelity GPR is presented in Section 2.1.2. The use of different co-variance functions such as constant, linear, squared exponential, Matern and rational quadratic, defines the method of prediction for the Gaussian process.

#### 2.1.1. Gaussian Process Regression (GPR)

GPR is a non-parametric, stochastic process that follows the Bayesian approach for regression, working well on small data sets and having the ability to provide uncertainty measurements on predictions. Predictions are derived using a probability distribution over all possible values of a time-series using prior functions $w$ of training points $f$ at observed points $t$, and targeted values $f^*$ at unobserved points $t^*$ are calculated from a predictive distribution, $p(f^*|t^*, f, t)$, by considering all possible predictions using their calculated posterior distribution [14]:

$$p\left(f^*|t^*, f, t\right) = \int p\left(f^*|t^*, w\right) p\left(w|f, t\right) dw. \tag{1}$$

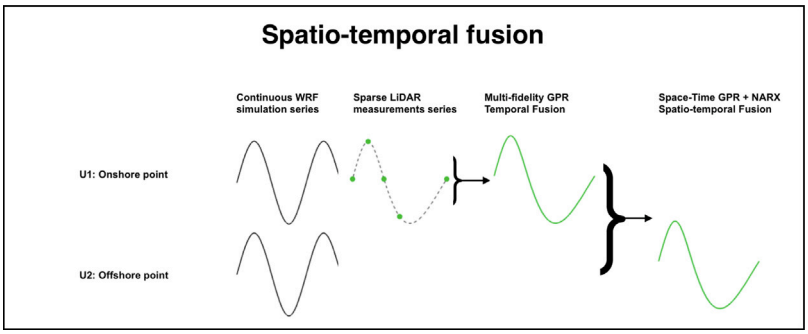


**Fig. 1.** Flow chart for spatiotemporal fusion. U1 and U2 represent the wind speed at an onshore and offshore positions, respectively.

To trace the integration process of Eq. (1), all terms of the equation are assumed Gaussian. The prior function defines the Gaussian distribution [14]:

$$f(t) \sim GP(m, k(t, t')), \tag{2}$$

where $m$ is the mean function, which represents the trend of the function, and the covariance function (kernel), $k(t, t')$, represents the dependence of the structure, defined by the hyperparameters [15].

#### 2.1.2. Multi-fidelity Gaussian process regression

In this section, we discuss advanced temporal data fusion using data with multiple fidelities to enhance the accuracy of prediction. The data sets are obtained using different techniques mathematically, the multi-fidelity technique considers the high-fidelity model as a function of two variables $(t, s)$ and then uses the low-fidelity data as the $s$ variable [14]:

$$f_h(t) = g(t, f_1(t)), \tag{3}$$

where in the present work $f_h(t)$ and $f_l(t)$ are the high-fidelity LiDAR measurements and low fidelity WRF simulations, respectively. Such non-linear auto-regressive Gaussian process (NARGP) has been observed to produce highly accurate prediction when $f_h(t)$ is non-linearly dependent on $f_l(t)$, and GPR is then performed in a two-dimensional space.

To implement this, we adopt the co-kriging model, which uses multivariate functions with respect to different levels of fidelities to reflect different accuracies. The additional data set is later introduced to the Gaussian distribution and we add the terms of the first data set $(t, s)$ and the second data set $(t', s')$ while the mean function is zero, through [14]:

$$f(t) \sim GP(m, k((t, s), (t', s'))). \tag{4}$$

Merging of two or more sets that are approximately linearly dependent by scaling and shifting parameters was approached by Kennedy and OHagan [16]. However, due to the presence of nonlinear dependencies generally between the data sets, the quality of results degraded as a major issue for linear data fusion algorithms. To overcome and resolve the nonlinear dependencies, space-dependent scaling factor $\rho(x)$ [14] or alternatively, deep multi-fidelity GP [17] was introduced. Yet the improvement brings further optimizations of additional hyperparameters. Here the NARGP algorithm, an implicit automatic relevance determination (ARD) weight, is employed in the extended space, parametrized by $t$ and $s$, which counts as a different scaling of the existing hyperparameters for each dimension in the kernel [18].

Additionally, the formulation can be extended through functions of the low-fidelity data set. The high-fidelity data can be further considered as a function $t$, $f_l(t)$ and the derivatives of $f_l(t)$, exploiting that $f_l(t)$ has a similar trend with $f_h(t)$ [14]:

$$f_h(t) = g(t, f_l(t), f_l^1(t), \ldots, f_l^i(t)), \tag{5}$$

where $f_l^i(t)$ is the $i$th derivative of the low fidelity data.

### 2.2. Spatial extrapolation

As aforementioned the target is to predict offshore wind indirectly from onshore measured wind. Therefore apart from the temporal fusion algorithms presented above, a spatial extrapolation is required. Here a time series neural network is adopted to link the wind speed at the two points using a single variable nonlinear network NAR along with NARX to have a fair performance comparison. In practice, low-fidelity WRF data will be used to train the network and onshore hybrid solution (obtained by temporal fusion) is served as input to estimate the offshore wind.

#### 2.2.1. Nonlinear Autoregression (NAR)

The NAR model is most suitable for time-series predictions where the main source of training data is only past values of the time series itself, and this process is called feedback delays. The network is trained in an open loop, which uses the real target values as a response. Following, the network becomes a closed-loop, and the predicted values are used as new response inputs to the network. The framework of this model is seen in Fig. 2(*a*), a multi-layer network where the left hand side is the past delayed input values $y(t-1), y(t-2)$, and $y(t-p)$ is used to obtain the independent variable $y(t)$. Optimization of the network aims to reduce the number of synapses (weights) and neurons, and subsequently reducing the complexity of the network, and maintaining the generalization capabilities.

#### 2.2.2. Nonlinear Autoregression with External Input (NARX)

NARX is a dynamically guided type of recurrent ANN containing one or more feedback loops. The loops can be either local or regional, and the use of regional loops enables a significant reduction of memory. Recurrent networks are being used for two main functional tasks, first, for associative memory tasks and second, for input–output mapping networks. The applications of input–output mapping networks include modelling and signal predictions for time-series [19]. The learning algorithm for the NARX network is based on the performance function used in the training of ANN, which is the mean squared error (MSE). NARX neurons are sigmoid and the performance function is derived to include a mean squared weight function with a performance ratio. As a result, the performance function operates under smaller weights and biases, thus causes the network response to be much smoother and less likely to over fit.

Learning in NARX networks is more efficient and effective than in other neural networks, since it has a better descending gradient, which leads to much faster convergence and better generalization than other networks. The model predicts a series $y(t)$ given specific past values of $y(t)$ and an additional input series $x(t)$ as shown in Fig. 2(b), where the NARX architecture is illustrated. The model has only one input, the exogenous variable $x(t)$, providing feed-forward to a $q$ delayed memory neurons, and one output, $y(t+1)$, which is the value of the predicted variable one step ahead. Dynamically, this can be expressed by [11]:

$$y(n+1) = F(y(n), y(n-q+1), u(n), u(n-q+1)), \tag{6}$$

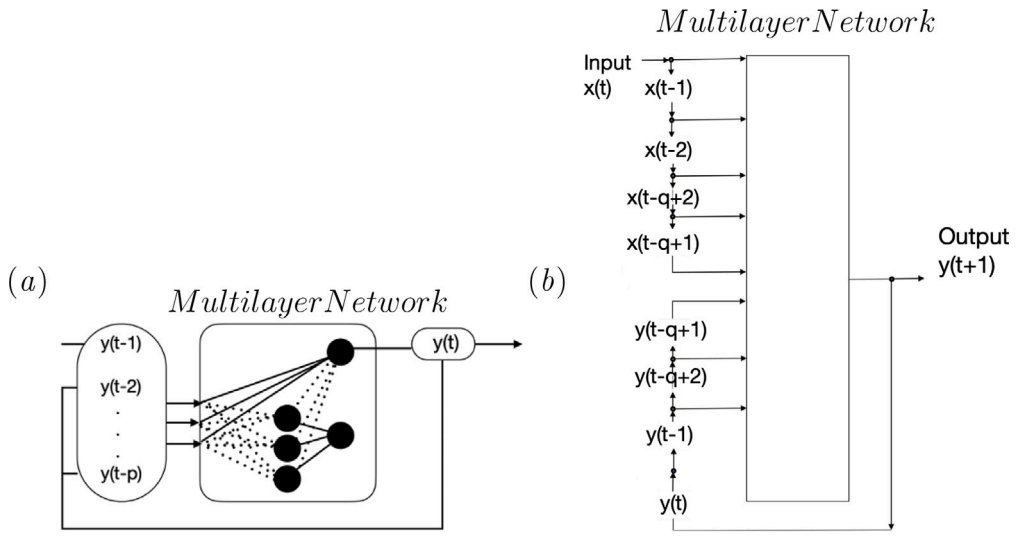


**Fig. 2.** (*a*) Architecture of the NAR (nonlinear autoregressive) model with a multi layer perception. (*b*) Framework for NARX model with an exogenous variable $x$ as the input. $q$ past values of $x$ and $y$ are considered for the prediction of $y(t+1)$.

Since the input is one step behind the output with respect to time, the output can provide feedback to the network through the delayed memory neurons, which in turn makes up the input neural layer of a multilayer network.

The learning algorithm for the NARX network is based on the performance function used in the training of ANN, which is the mean squared error (MSE). NARX neurons are sigmoid and the performance function is derived to include a mean squared weight function with a performance ratio. As a result, the performance function operates under smaller weights and biases, thus causes the network response to be much smoother and less likely to over fit.

As it was proven essential to have at least two-thirds of the data for training, the data is partitioned to 60, 20 and 20 percents for training, validation and testing, respectively. We constructed 10 hidden neurons with 2 delays, and adopted the Bayesian regularization as the training algorithm which trades off more computational costs for better accuracy [11].

## 3. Case description

To test the methods, we consider a case associated with the RUNE project, which was a near-shore experiment conducted at the west coast of Denmark (see Fig. 3(*b*)). The surrounding area is nearly flat coastal farmland and moving northwards from position 1 to 3, the sand embankment separating the North Sea and the grasslands transforms into cliffs covered by grass. In this work, we use dual-Doppler scans performed nearly perpendicular to the coast from about 5 km offshore to 2 km onshore. These scans were performed by synchronizing measurements from two scanning LiDARs, which are modified versions of WLS200S Leosphere units, one located at position 1 and the other at position 3. Here, we use the dual-Doppler scans performed at 50 m above mean sea level (amsl) during the period 2015-12-08 to 2016-02-17. Due to filtering of high noise/low signal strength and system availability, only 114 10-min are available at all the dual-Doppler positions shown as black markers in Fig. 3(*a*). Further details with regards to the experimental campaign and the instrumentation can be found in [20].

Here we use a numerical experiment, which was part of a number of numerical simulations performed using the WRF model v3.6 to supplement the measurements of RUNE [21]. This particular experiment was setup with 4 nested domains, the outermost covering northwestern Europe and a 2-km horizontal resolution innermost domain covering the west coast of Denmark. Spectral nudging to the ERA5 reanalysis is used in the upper model levels of the outermost domain. The simulation had 8 vertical levels within the first 100 m and instantaneous output was produced every 10 min. The experiment also used the Mellor–Yamada–Janjic planetary boundary layer scheme, a sea surface temperature product from the Danish Meteorological Institute [22], and the CORINE land cover description. An illustration of the low fidelity WRF simulation data set of the most onshore point can be seen in Fig. 4(*a*), while Fig. 4(*b*) shows the high fidelity LiDAR measurements for the same point.

## 4. Data preprocessing

EWT is a three-model decomposition algorithm used in forecasting, and has been used to achieve good forecasting results for non-stationary time series such as wind speed series [8]. EWT can extract meaningful information from the series by designing appropriate wavelet filter banks. In our study, pre-processing of the WRF time series generated by ERA-5 can adaptively represent the processed signal by generating the adaptive wavelet and then decomposing the signal into a finite number of modes as per previous literature. The algorithm is based on identifying and extracting the different intrinsic modes of a time-series, by relying on robust pre-processing for peak detection, and then performs spectrum segmentation based on detected maxima to construct a corresponding wavelet filter bank.

The WRF series that were pre-processed using EWT are 1) the WRF series at the most onshore point used in Hybrid (3) of the Multi-fidelity GPR in Fig. 5, panel (c), and 2) the WRF series for the 36 points generated by the dual-Doppler scans used for Hybrid (3) in Fig. 6.

The process can be divided into five steps [8]:

1. Extending the signal.
2. Fourier transforms.
3. Extracting boundaries.
4. Building a filter bank.
5. Extracting the sub band.

The original wind speed signal had considerable high-frequency fluctuations. The three-level decomposition attained by the EWT algorithm describes the wind speed series in a meaningful way. Three uncorrelated filter modes were extracted from the wind speed series and a residual was also obtained from the extraction. The reconstructed wind speed series shows a significant decrease in fluctuations and will be served as input to the third GPR model.

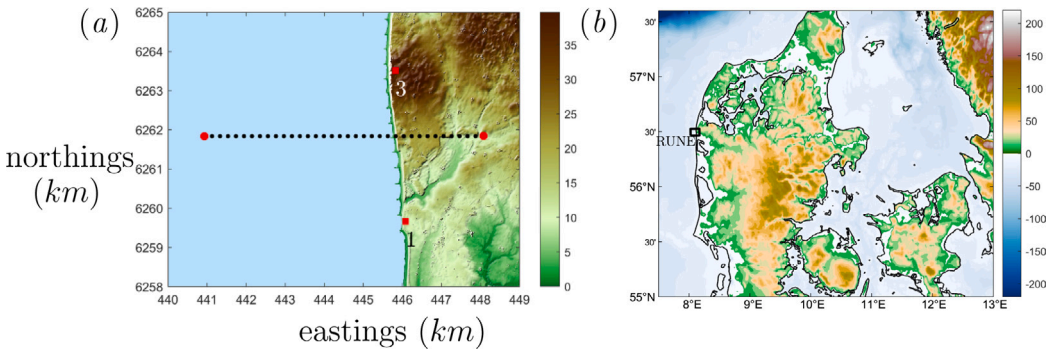


**Fig. 3.** (*a*) RUNE experimental area. Positions of the LiDARs are shown in red square markers and the dual-Doppler scans in black and red dot markers. The colour bar indicates the terrain elevation in metres above mean sea level. (*b*) The location of the RUNE experiment (black rectangle) in Denmark.

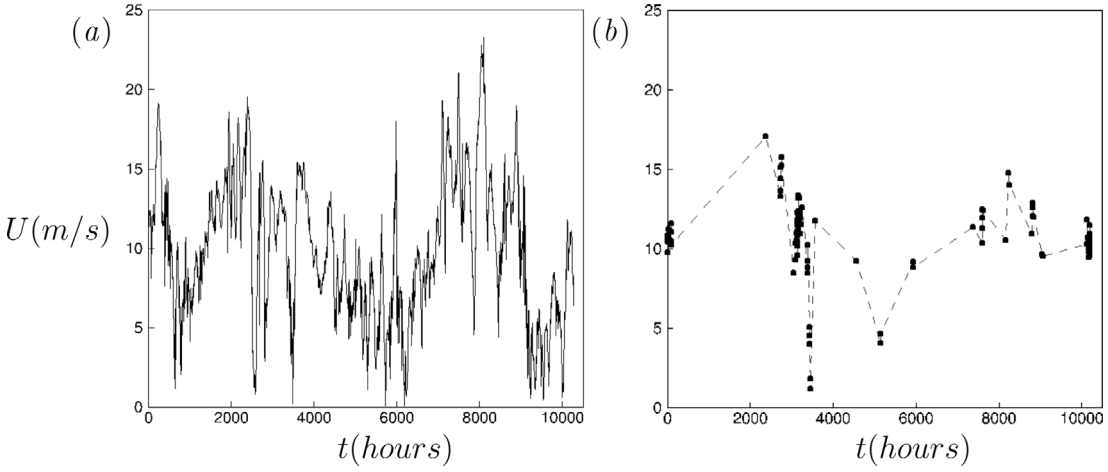


**Fig. 4.** (*a*) Low-fidelity data from numerical simulation (WRF) at the most onshore point, (see Fig. 3). (*b*) High-fidelity data from the dual-Doppler LiDAR setup at the most onshore point, (see Fig. 3).

**Table 1**
Configurations and accuracy of the GPR models.

| Model | Basis and Kernel functions | RMSE [m/s] |
|---|---|---|
| WRF | – | 1.24 |
| Hybrid (1) | Zero, Matern 5/2 | 1.15 |
| Hybrid (2) | Constant, Rational quadratic | 1.01 |
| Hybrid (3) | Zero, Matern 3/2 | 0.86 |

## 5. Results

### 5.1. Temporal data fusion

The different data sets at the furthest onshore point of the dual-Doppler line were merged by applying MF-GPR. The performance of the three models was optimized, through the hyperparameters, by applying 30 iterations of basis and kernel function combinations, including: Zero, Linear, Constant and Matern 5/2 and 3/2; Rational Quadratic, squared Exponential, etc. Firstly, we explored the original model, represented as Hybrid (1), where the input information was low and high-fidelity data sets. Then, we showed that introducing additional information sets, which are functions of the low fidelity data set (first and second derivatives) can enhance the accuracy of predictions, hence Hybrid (2). The third model, Hybrid (3), involved pre-processing of the training set using the EWT reconstruction algorithm, the regenerated first and second derivative sets of the low fidelity data, and finally the North and East decomposed wind speed vector components. A higher drop in RMSE was noted from the Original WRF data.

Table 1 shows the configuration and performance of NAR and NARX for the training of the network. The highest performing NAR and NARX configurations consisted of 3 delays, 15 neurons and 4 delays, 12 neurons, respectively, which implied that the latter required less statistic training. Despite hiring a lower number of neurons, the NARX network required less computation time to outperform the NAR network by 12%.

Fig. 5(*a*), (*b*) and (*c*) show the time series of the results from the three hybrid models, respectively. Hybrid (1) showed a 9% decrease in RMSE from WRF data, in Hybrid (2) the RMSE was reduced by about 18%, and finally Hybrid (3) showed the largest drop compared to other hybrid models, about 31%. Besides, panel (*d*) reflected a cut off to the interval between the hours 500–600 since the start of the experiment, with an 80% confidence interval, showing a better visualization of the performance. Finally, panel (*e*) presents the deviation error between the provided high-fidelity time series of 114 points with their predicted counterparts by the hybrid techniques. It can be seen that for some points, Hybrids (1) and (2) outperform each other with deviations ranging from 6 to 2 m/s. On the other hand, the performance of Hybrid (3) outperformed the other two at almost all measured points with the deviation capped at 2 m/s and mean deviation 0.6 m/s. These results substantiate that increasing the number of additional sets and pre-processing the data enhanced the accuracy of the Gaussian process [14].

Furthermore, we evaluate the performance of the hybrid methods against the software Windographer, the leading industrial software for importing, visualizing and analysing wind resource data. Windographer follows the Measure–Correlate–Predict (MCP) algorithms including Linear Least Squares (LLS); the method is on correlating

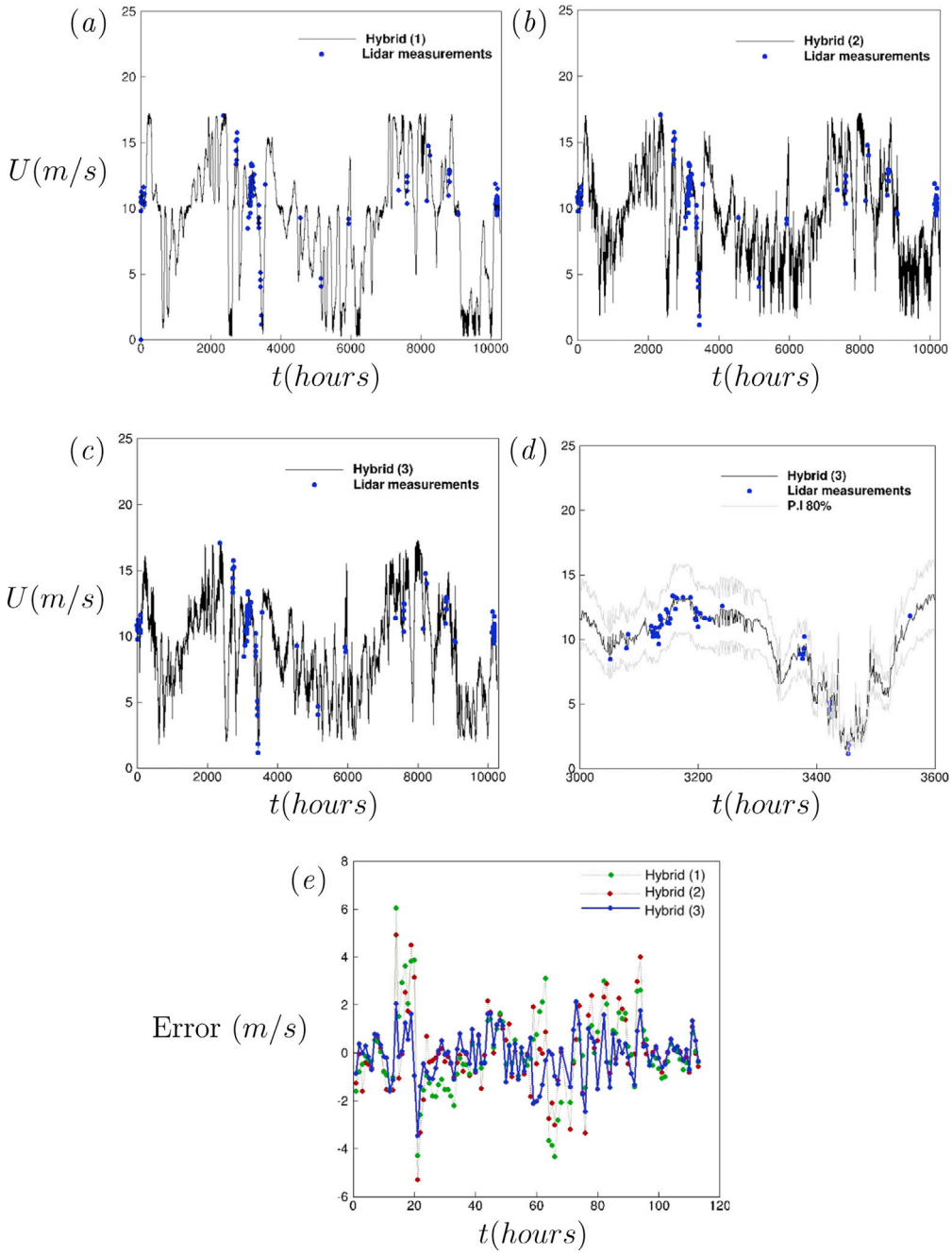


**Fig. 5.** (*a*), (*b*) and (*c*) represent temporal data fusion results for Hybrids (1), (2) and (3), respectively. (*d*) Cut-off panel for Hybrid (3) from 500 to 600 h of the experiment and (*e*) Error in all three hybrid models against 114 LiDAR measurements.

target and reference speed data, based on the linear least squares procedure. The RMSEs for each of the 36 dual-Doppler points from the furthest offshore point to the most onshore one using all 3 hybrid methods and the industrial software are shown in Fig. 6.

On average, Hybrids (1), (2), and (3) were able to perform 12%, 14%, and 60%, respectively, more accurate than the industrial software. In addition, the hybrid methods showed a higher consistency in predictions that occurred offshore, where the industrial software had a relatively poor performance. Moreover, the highest RMSE for the hybrid methods was observed at 446 km easting, where the transition from offshore to onshore takes place. On the other side the industrial software was not affected, and the performance of the predictions was consistent.

### 5.2. Spatial data fusion

The spatial data fusion aimed to project the onshore measurements to offshore locations in light of numerical simulations, to reduce the cost of direct offshore measurements. The first and last offshore and onshore points in the 36 dual-Doppler line were considered as an example. An ANN was trained using the low-fidelity WRF data at both points, and it configured the winds relation at both points. The network was later tested on the high-fidelity LiDAR data of the onshore point and generated high fidelity wind speed results for the offshore point [15].

For the NARX model, eleven simulations were performed varying the number of past values (delays) for the entry variables from 1 to

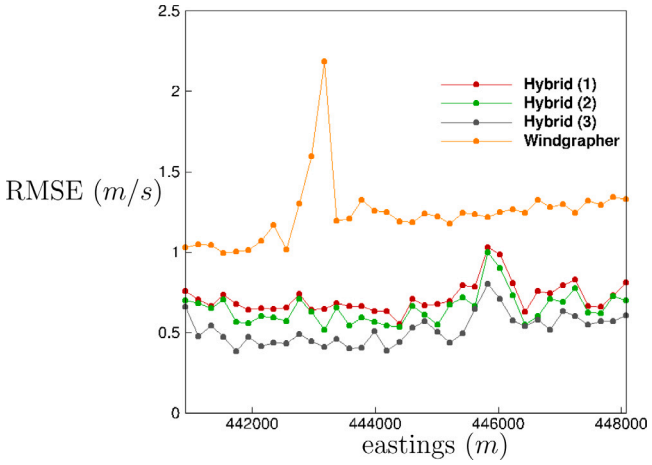


**Fig. 6.** RMSE curve across Windographer and all three hybrid models for all 36 dual-Doppler points.

10, and the number of hidden neurons from 3 to 21. The MSE of the test data set was used to assess the performance of the network, the configuration with the best performance was employed. The same number of simulations were carried for the NAR model; similarly, the past values varied from 1 to 10 and the hidden neurons from 3 to 15 and the configuration with the lowest MSE was selected.

Table 2 shows the configuration and performance of NAR and NARX for the training of the network. The highest performing NAR and NARX configurations consisted of 3 delays, 15 neurons and 4 delays, 12 neurons, respectively, which implied that the latter required less statistic training. Despite hiring a lower number of neurons, the NARX network required less computation time to outperform the NAR network by 12%.

Fig. 7(*a*) shows the results from testing the NARX network using the LiDAR measurements along with low-fidelity WRF data and high-fidelity LiDAR measurements of the most offshore point. Predicted values from the network were more accurate than the low-fidelity data, where the RMSE was reduced from 1.23 m/s to 1.17 m/s. For a zoomed-up visualization of results, the data-rich high-fidelity section at hours 500–600 is shown in Fig. 7(*b*).

### 5.3. Spatio-temporal extrapolation

In this section, we combined temporal and spatial data fusion using 1331 10 min LiDAR measurements. The aim was to use the intermittent

**Table 2**
Configurations of the NARX and NAR Networks with the Best Performance.

| Model | Delays and Neurons | Time steps | MSE ($\times 10^{-2}$) |
|---|---|---|---|
| NAR | 3, 15 | Training (6176)<br>Validation (2058)<br>Test (2058) | 1.352<br><br>1.559 |
| NARX | 4, 12 | Training (6176)<br>Validation (2058)<br>Test (2058) | 1.241<br><br>1.188 |

measurement at the second most onshore point to estimate the wind at the most offshore point by exploiting the numerical data.

Temporal data fusion was performed following the same technique as Hybrid (3) of MF-GPR from Section 2.1.2, we used the reconstructed set from the EWT algorithm for pre-processing and five predictors for the GPR algorithm: low-fidelity WRF data, first and second derivatives, North and East vector components of the wind speed set of the onshore point. Again, 30-iterations were used to optimize the hyperparameters, varying the basis and kernel functions to achieve a configuration with an RMSE of 0.84 m/s.

Following, a NARX neural network was trained using the low-fidelity WRF data of both the second most onshore and most offshore points with 3 delays and 12 hidden neurons. The network was later tested on the time series generated from the temporal section using MF-GPR and the performance of the network was estimated at an MSE of $1.12 \times 10^{-2}$.

Fig. 8(*a*) shows the final curve of the spatial–temporal data fusion process, high-fidelity LiDAR data (hidden in the assessment), and 80% prediction intervals. In addition, Fig. 8(*b*) is a cut-off to show the region with the richest LiDAR data, the results were satisfactory, as it achieved an accurate result with an RMSE 1.23 m/s impersonating the high-fidelity data of the most offshore point without discontinuity or using expensive LiDARs offshore. These results outperformed the WRF simulation at the offshore location where the RMSE was 1.46 m/s.

## 6. Conclusions

In this work, we performed data fusion of numerical model results from WRF simulations (low fidelity), continuous in space and time with LiDAR measurements sparse in time and space (high fidelity) to obtain a spatial–temporal extrapolation, suitable for the assessment of offshore wind. The RUNE experiment performed dual-Doppler scans which generated 114 10-minute measurements over three months for the present spatial-only and temporal-only data fusion, and 1331 10-minute measurements for the present spatiotemporal experiment. Simultaneously,

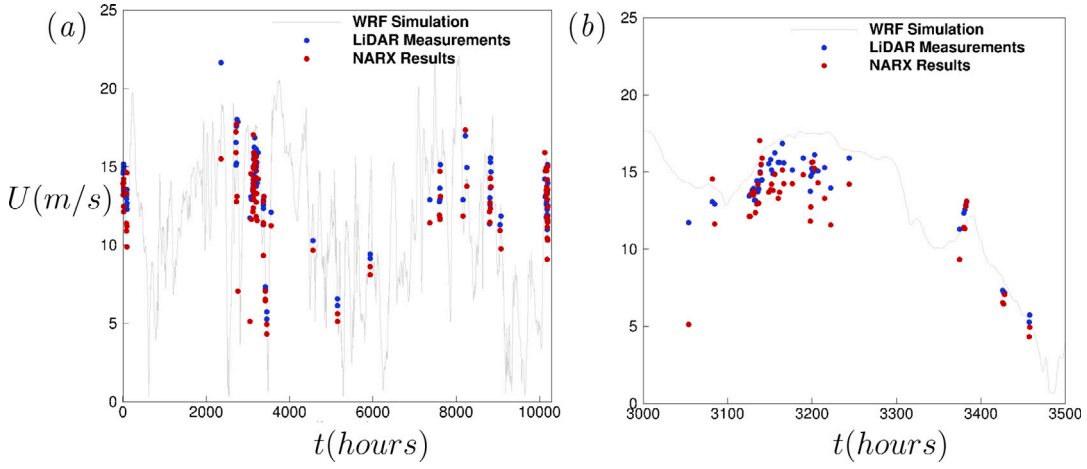


**Fig. 7.** (*a*) Spatial data fusion results for the offshore point. (*b*) Close-up of spatially predicted data and high and low-fidelity data for validation.

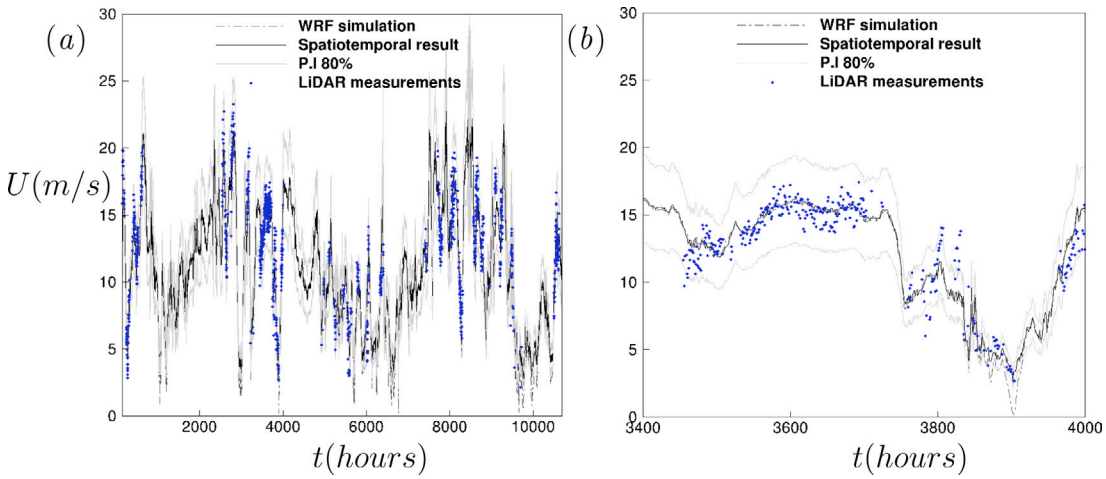


**Fig. 8.** (*a*) Response for Spatio-temporal data fusion. (*b*) Close-up of the final spatiotemporal results ranging from hours: 3400–4000.

numerical simulations performed using the WRF model v3.6 generated an instantaneous output every 10 min for the same period of 3 months.

For time-domain data fusion, we were able to represent the high-fidelity data at unobserved regions and periods by exploiting the low-fidelity data and its functions. The addition of extra information data sets (derivatives and wind speed vector components) and pre-processing showed an improvement in the prediction performance in terms of RMSE, with a 30% average drop compared to other models that ignored them. For the spatial fusion part of the experiment, similarly, adding extra information data sets to the NARX neural network showed improvements compared to the single input model NAR. The data from the network had a lower MSE for assessing offshore data, which could avoid sending expensive equipment offshore.

Following data fusion in both space and time, the models were re-run at the optimized configuration of each method: Data from the second most onshore point underwent Hybrid (3) MF-GPR for time-domain data fusion, and the continuous time series output was used along with data from the offshore point for space domain data fusion. Finally, the spatial–temporal data fusion resulted in accurate offshore wind resource assessments within a 2% margin error for wind speed.

There are two major limitations in this study that could be addressed in future research. First, the study focused on data obtained from the RUNE experiment, which included only 1331 measured points from LiDAR equipment equivalent to 220 h of measured data, scattered across the entire 3 months period of the experiment, which means a lot of weeks are empty. On the other side, the WRF simulation covered the entire duration with almost 10,500 points. This limited access to high-quality data is a result of low availability of LiDARs, which is due to the harsh weather conditions offshore that often damage the equipment. The rareness of LiDAR data can influence the GPR, which makes it harder to captures trends and meaningful relations.

Second, the most onshore and offshore points of the 36 dual-Doppler were selected from the experiment. However, due to the low resolution of WRF (2 km), interpolation is necessary to obtain WRF data at corresponding points, which reduces the accuracy of predictions.

Future work also concerns further development to the multi-fidelity data fusion algorithm, by introducing additional sources of data generated by different equipment or software. An example of this is the use of a second WRF simulation with different resolutions and features. Nevertheless, concerning the results for one point-based prediction, we can also expect to perform 3-dimensional area predictions with respect to time, by performing data fusion of multiple LiDAR measurements at different locations with full grid WRF simulation results.

## CRediT authorship contribution statement

**Basem Elshafei:** Performed the data fusion work, Writing - original draft. **Alfredo Peña:** Processed the LiDAR data and drafted the LiDAR part of the manuscript. **Dong Xu:** Ran the Windgrapher tests for comparison with the proposed method. **Jie Ren:** Designed the data structure to be fused. **Jake Badger:** Performed the WRF study. **Felipe M. Pimenta:** Co-wrote the data processing part of the manuscript. **Donald Giddings:** Co-wrote the Gaussian process method. **Xuerui Mao:** Coordinated the work and summarized the findings.

## Declaration of competing interest

The authors declare that they have no known competing financial interests or personal relationships that could have appeared to influence the work reported in this paper.

## Acknowledgements

This project has received funding from the European Union Horizon 2020 research and innovation programme under the Marie Skodowska-Curie grant agreement No 777717 and the future and emerging technologies programme with agreement No. 828799.

## References

[1] Negnevitsky M, Johnson P, Santoso S. Short term wind power forecasting using hybrid intelligent systems. 2007.
[2] Hoolohan Victoria, Tomlin Alison S, Cockerill Timothy. Improved near surface wind speed predictions using Gaussian process regression combined with numerical weather predictions and observed meteorological data. Renew Energy 2018;126.
[3] Murthy KSR, Rahi OP. A comprehensive review of wind resource assessment. Renew Sustain Energy Rev 2017;72.
[4] Sempreviva AM, Barthelmie RJ, Pryor SC. Review of methodologies for offshore wind resource assessment in European seas. Surv Geophys 2008;29.
[5] Singh Shikha, Bhatti TS, Kothari DP. A review of wind-resource-assessment technology. J Energy Eng 2006;132.
[6] Zhang Chi, Wei Haikun, Zhao Xin, Liu Tianhong, Zhang Kanjian. A Gaussian process regression based hybrid approach for short-term wind speed prediction. Energy Convers Manage 2016;126.
[7] Soman Saurabh S, Zareipour Hamidreza, Malik Om, Mandal Paras. A review of wind power and wind speed forecasting methods with different time horizons. 2010.
[8] Hu Jianming, Wang Jianzhou. Short-term wind speed prediction using empirical wavelet transform and Gaussian process regression. Energy 2015;93.
[9] Kandasamy Kirthevasan, Dasarathy Gautam, Oliva Junier, Schneider Jeff, Póczos Barnabás. Multi-fidelity Gaussian process bandit optimisation. J Artificial Intelligence Res 2019;66.

[10] Tastu Julija, Pinson Pierre, Kotwa Ewelina, Madsen Henrik, Nielsen Henrik Aa. Spatio-temporal analysis and modeling of short-term wind power forecast errors. Wind Energy 2011;14.
[11] Cadenas Erasmo, Rivera Wilfrido, Campos-Amezcua Rafael, Cadenas Roberto. Wind speed forecasting using the NARX model, case: La mata, oaxaca, México. Neural Comput Appl 2016;27.
[12] Liu Jingwen, Gu Yanlei, Kamijo Shunsuke. Customer pose estimation using orientational spatio-temporal network from surveillance camera. Multimedia Syst 2018;24.
[13] Dalmau Ramon, Pérez-Batlle Marc, Prats Xavier. In *Estimation and prediction of weather variables from surveillance data using spatio-temporal Kriging, Vol. 2017-September, 2017*.
[14] Higdon Dave, Picard Dominique, Parussini L, Venturi D, Perdikaris P, Karniadakis GE. Multi-fidelity Gaussian process regression for computer experiments Thèse dirigée par Josselin Garnier Thèse rapportée par. J Comput Phys 2017;336.
[15] Alamaniotis Miltiadis, Karagiannis Georgios. Integration of Gaussian processes and particle swarm optimization for very-short term wind speed forecasting in smart power. Int J Monit Surveillance Technol Res 2018;5.
[16] Kennedy MC, O'Hagan A. Predicting the output from a complex computer code when fast approximations are available. Biometrika 2000;87.
[17] Perdikaris P, Raissi M, Damianou A, Lawrence ND, Karniadakis GE. Nonlinear information fusion algorithms for data-efficient multi-fidelity modelling. Proc R Soc A 2017;473.
[18] Rasmussen Carl Edward, Williams Christopher KI. Gaussian processes for machine learning. 2018.
[19] Li Yunhua, Ling Lina, Chen Jiantao. Combined grey prediction fuzzy control law with application to road tunnel ventilation system. J Appl Res Technol 2015;13.
[20] Floors Rogier, Peña Alfredo, Lea Guillaume, Vasiljević Nikola, Simon Eliot, Courtney Michael. The RUNE experiment-a database of remote-sensing observations of near-shore winds. Remote Sens 2016;8.
[21] Floors R, Hahmann AN, Peña A. Evaluating mesoscale simulations of the coastal flow using lidar measurements. J Geophys Res: Atmos 2018;123.
[22] Høyer Jacob L, Karagali Ioanna. Sea surface temperature climate data record for the north sea and baltic sea. J Clim 2016;29.